Available online at www.sciencedirect.com
ScienceDirect
PERGAMON
Acta Astronautica 64 (2009) 1264–1275
ACTA ASTRONAUTICA
www.elsevier.com/locate/actaastro

Aerospike nozzle contour design and its performance validation

Chang-Hui Wang*, Yu Liu, Li-Zi Qin

403 Teaching and Research Section, Beijing University of Aeronautics and Astronautics, 100083 Beijing, People's Republic of China

Received 13 March 2007; accepted 8 January 2009
Available online 20 February 2009

A simplified design and optimization method of aerospike nozzle contour and the results of tests and numerical simulation of aerospike nozzles are presented. The primary nozzle contour is approximated by two circular arcs and a parabola; the plug contour is approximated by a parabola and a third-order polynomial. The maximum total impulse from sea level to design altitude is adopted as objective to optimize the aerospike nozzle contour. Experimental studies were performed on a 6-cell tile-shaped aerospike nozzle, a 1-cell linear aerospike nozzle and a 3-cell aerospike nozzle with round-to-rectangle (RTR) primary nozzles designed by method proposed in present paper. Three aerospike nozzles achieved good altitude compensation capacities in the tests and still had better performance at off-design altitudes compared with that of the bell-shaped nozzle. In cold-flow tests, 6-cell tile-shaped aerospike nozzle and 1-cell linear aerospike nozzle obtained high thrust efficiency at design altitude. Employing gas H_2/gas O_2 (GH_2/GO_2) as propellants, hot-firing tests were carried out on a 3-cell aerospike nozzle engine with RTR primary nozzles. The performance was obtained under two nozzle pressure ratios (NPR) lower than design altitude. Efficiency reached 92.0–93.5% and 95.0–96.0%, respectively. Pressure distribution along plug ramp was measured and the effects of variation in the amount of base bleed on performance were also examined in the tests.
© 2009 Elsevier Ltd. All rights reserved.

Keywords: Rocket propulsion; Aerospike nozzle; Contour; Experiment; Performance

1. Introduction

A high efficient propulsion system is one of the key factors to realize an advanced launching vehicle. Research and development of reusable propulsion system characterized by lightweight, low cost and high performance is the inevitable trend of future aerospace propulsion technology. The rocket engine with bell-shaped nozzle has been brought to its full development up to now and it is difficult to essentially improve its performance to a great extent. Compared with conventional rocket engine, aerospike nozzle engine characterized by small scale, lightweight, high performance during all altitudes and better utilization of the vehicle base is the promising candidate for the propulsion device of future advanced launching vehicle. Aerospike nozzle technology is the key technology of aerospike nozzle rocket engine. Aerospike nozzle is a type of nozzle with capacity of continuous altitude compensation. Aerospike nozzle is considered to have better performance at off-design altitudes compared with that of the conventional bell-shaped nozzle since its plume is open to the atmosphere outside and free to adjust, allowing the engine to operate at its optimum expansion at all altitudes.

The aerospike nozzle engine was once a candidate for the space shuttle propulsion and had been studied from the early 1960s until the end of the 1970s. However, technological difficulties in the development of the aerospike nozzle made it fall behind the development of conventional nozzle and research on the aerospike nozzle stagnated. In the 1990s, much attention was

* Corresponding author.
E-mail address: wangchanghui@buaa.edu.cn (C.-H. Wang).

0094-5765/$ - see front matter © 2009 Elsevier Ltd. All rights reserved.
doi:10.1016/j.actaastro.2008.01.045

Nomenclature

a, b, c, d	coefficients of geometric curves
A	area
C_F	thrust coefficient
D	height or diameter
F	thrust
L	length
M	Mach number
NPR	P_c/P_a, nozzle pressure ratio
P	pressure
R	radius
R_g	gas constant
T	temperature
V	velocity
W	width of the plug
x, y	Cartesian coordinates
α	primary nozzle inclination
β	mixing ratio
θ	angle
ε	area ratio
η	thrust efficiency
$\dot{m}$	mass flow rate
ρ	density
γ	specific heat ratio

Subscripts

a	ambient
all	total
c	combustion chamber
e	primary nozzle exit
ep	plug exit
p	plug
t	throat
td	throat downstream
tu	throat upstream
H	hydrogen
O	oxygen

devoted to this nozzle concept and intensive studies on the aerospike nozzle were carried out again in the United States [1,2], Europe [3], Japan [4,5], Russia [6,7] and China [8]. Because of overweight composite cryogenic fuel tank and high cost, X-33 vehicle plan was called off eventually, however, full-size linear aerospike engine was produced and hot-firing tested at sea level successfully. Up to now, investigation and applications on aerospike nozzle in small scale are still in progress [9].

The investigation on aerospike nozzle has been carried out in China since 1997. The activities concerned include contour design and its optimization [10], both hot-firing and cold-flow tests and numerical simulations [11,12]. Tile-shaped aerospike nozzle was proposed and its primary performance validation was done by hot-firing test [13]. Flowfield [14], base behavior [15] as well as effects of free stream on flowfield and performance of aerospike nozzle [16] were also studied by either experiments or numerical simulations in China. In present paper, design and optimization of the aerospike nozzle contour was discussed and performance validation was carried out by cold-flow and hot-firing tests.

2. Contour design and optimization

In 1964, an approximate design method of the aerospike nozzle was proposed by Angelino [17]. This method is based on the assumptions that the exhaust properties at the plug inlet are uniform and one-dimensional, so that the expansion fan emanating from the external lip of the primary nozzle are straight lines and properties along each expansion wave are uniform. On these assumptions, the aerospike nozzle (with primary nozzle area ratio $\varepsilon_c = 1$) contour depends only on specific heat ratio γ and total area ratio ε_{all}. An aerospike nozzle contour designed by Angelino method is called an ideal one, having perfect performance in uniform flowing condition, and has already been widely adopted [4,18,19]. However, a contour designed by Angelino method is a series of discrete points, so it is difficult to keep the profile drawn by these points continuous and smooth rigorously or optimize contour configuration for maximum overall performance. In order to design an aerospike nozzle contour quickly, correctly and efficiently, especially for the contour optimization, both primary nozzle and plug contours are approximated by simple geometric curves in this section. Describing these geometric curves by simple mathematical functions and finally obtaining the contour from geometric and aerodynamic restrictions seems to be a promising solution either for contour design or contour optimization.

2.1. Description of the primary nozzle contour

Contour design method developed for conventional bell-shaped nozzle also well adapts to the primary

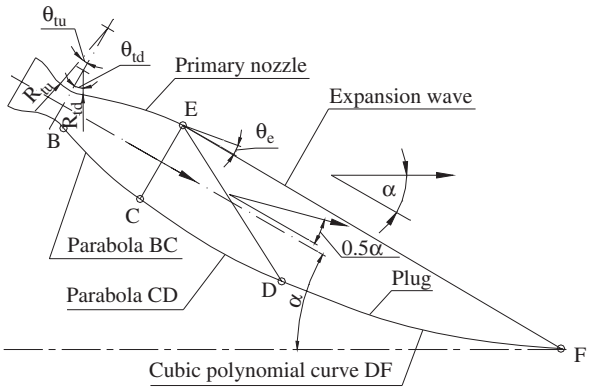

Fig. 1. Sketch of the full-length aerospike nozzle contour.

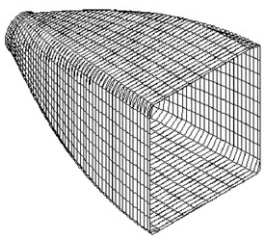

Fig. 2. Sketch of round-to-rectangle nozzle with transition from throat.

nozzle contour. For the axisymmetric or two-dimensional primary nozzle, two tangent circular arcs are assumed at throat region called upstream arc with radius R_{tu} and downstream arc with radius R_{td} (in Fig. 1). The divergent part of the primary nozzle contour BC is simply approximated by a parabola [20]; other contour parameters are central angle of the downstream arc θ_{td} and contour divergence angle θ_e at the primary nozzle exit. Generally, a primary nozzle contour can be determined by following three geometric restrictions. First at all, the starting point of parabola is fixed by R_{td} and θ_{td}. Secondly, the parabola slope at the starting point is fixed by θ_{td}. Finally, the parabola slope and radius (or height) at the primary nozzle exit are fixed by θ_e and ε_c, respectively.

For a round-to-rectangle (RTR) primary nozzle as shown in Fig. 2, the contour is converted from the bell-shaped nozzle. A conventional bell-shaped nozzle with the same throat radius and area ratio with RTR primary nozzle is designed first as a reference contour. The RTR contour cross section with the transition from RTR area is equal to the one of reference contour at the same axial distance from the throat. In transversal direction, the contour between the neighboring ribs is a circular arc. At the axial length where the contour starts to deviate from the round form, the radius R_1 is equal to the reference contour radius. At the exit, the circular arc radius is R_2. The arc radius is linear with distance from the place of initial deviation. Of course, other RTR methods can be developed including converting reference contour by other means. A RTR nozzle contour transiting from the round cross section at the throat to the square cross sections at the exit is shown in Fig. 2. Now, design and optimization of RTR primary nozzle contour is still under investigation and this must be done in combination of plug contour consideration.

2.2. Description of plug contour

Based on the curvefitting analysis, full plug contours designed by the method proposed by Angelino, can be described approximately by two mathematical curves like parabolic approximation for the bell-shaped nozzle contour and this contour modeling is necessary for the following contour optimization. The upstream contour CD is approximated by a parabola $y = a_1 + b_1x + c_1x^2$ and the downstream one DF is approximated by a third-order polynomial $y = a_2 + b_2x + c_2x^2 + d_2x^3$, two curves connect with each other at point D smoothly (Fig. 1). The position of connective point D is dependent of exhaust expansion. After some analysis of plug contours designed by Angelino method for different purposes, it is assumed in this paper that the exhaust deviation angle from primary nozzle axis after expansion wave ED is half of that after expansion wave EF under design condition.

Under design condition, expansion wave EF is the last one emanating from primary nozzle upper lip E. Passing EF, the exhaust pressure becomes equal to the ambient pressure at design altitude and the exhaust flows in the direction of aerospike nozzle axis (horizontal direction) with a total turning angle α. Thus, for mass conservation, the length L of EF can be determined by the density ρ, velocity V and Mach number M of exhaust behind the expansion wave EF with $L = \dot{m}M/\rho VW$, here, $\dot{m}$ is the mass flow rate and W is the width of the plug. Then, combined with the inclination of EF, coordinates of F can be obtained.

The turning angle of exhaust passing expansion wave ED is $\alpha/2$ and flow parameters along ED are achieved by Prandtl–Meyer function with the same way applied to EF, thus, the position of point D is also determined. Not only three critical points C, D and F are fixed but also tangent angles at points C and F are known, combined with connecting condition at point D, coefficients in parabola CD and the third-order curve DF are solved.

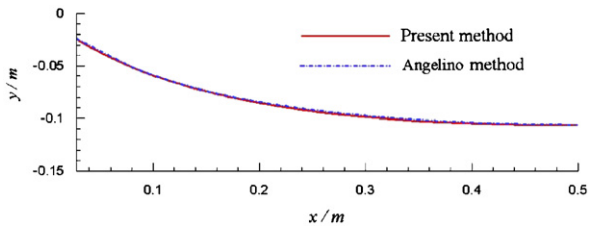

Fig. 3. Comparison of plug contours designed by two methods.

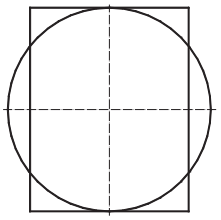

Fig. 4. Circular exit to 2-dimensional plug ramp inlet.

The plug contour description method discussed here is also developed from uniform one-dimensional assumptions. For an extension, if θ_e at the primary nozzle exit is considered, the primary nozzle declination α is described by $\alpha = \nu(M_{ep}) - \nu(M_e) - \theta_e$. Where, $\nu(M)$ is Prandtl–Meyer function; M_{ep} and M_e denote Mach numbers under design condition at full plug tip outlet and the primary nozzle lip E, respectively.

An aerospike nozzle contour is designed by the method stated above, with throat height $D_t = 4\,\text{mm}$, $\varepsilon_c = 4.0$ and $\varepsilon_{all} = 42.0$. Fig. 3 compares the plug contours designed by both Angelino method and the method presented in this paper. Two profiles almost coincide with each other and it is found that a plug contour modeled by two curves is reasonable and feasible.

A simple description of a two-dimensional plug contour is proposed above, for a tile-shaped plug contour, some additional disposals should be done first so as to use this design method. The axisymmetric distribution of exhaust properties at primary nozzle exit must be converted to two-dimensional distribution in the conditions that the plug inlet area and height are the same with the primary nozzle exit area and diameter, respectively, and the distribution of exhaust properties at plug inlet are the same with that at primary nozzle exit diameter (in Fig. 4) and then the width of the plug W is obtained.

2.3. Optimization of the full aerospike nozzle contour

An aerospike nozzle contour can be determined by D_t, R_{tu}, R_{td}, θ_{td}, θ_e, ε_c and ε_{all}. α is dependent on ε_{all} and ε_c and can be calculated from Prandtl–Meyer function. An optimized aerospike nozzle contour having maximum overall performance during flight can be achieved by proper selection of these geometric parameters. It was found that varied within a certain range, R_{tu} and R_{td} have slight influence on performance, so they were not adopted as design variables and $R_{tu} = 3R_t$, $R_{td} = R_t$ are always designated. ε_{all} and D_t are determined before contour design, so ε_{all} and D_t were not adopted as design variables also. γ and gas temperature in primary nozzle combustion chamber T_c is determined by thermochemical calculation. That is to say, only θ_{td}, θ_e and ε_c were adopted as optimization variables here.

Considering optimum overall performance of an aerospike nozzle during the whole flying trajectory, the maximum total impulse from sea level to design altitude is selected as an objective. For simplicity, total impulse is computed under following assumption that

(1) Flying trajectory is vertical.
(2) External flow effects are neglected during flight.
(3) Gas pressure and temperature in the primary nozzle combustion chamber keep constant during operation at all altitudes.
(4) Aerodynamic drag is only the function of flying velocity and aerospike nozzle effective sectional area.

For its advantage of fast operating speed, the method of characteristic was utilized to compute the performance of the aerospike nozzle. But, it is difficult to obtain the objective as a function of design variables directly in a certain form of formula. So the contour optimization was achieved by enumeration of design variables, namely design variables were given in discrete value within reasonable ranges and performances of the aerospike nozzle designed by different combinations of these discrete values were computed and compared. After all the combinations were computed and compared, the optimum values for design variables were obtained. Theoretically speaking, the best aerospike nozzle contour can be concluded by this enumeration method, provided that the discrete nodes of variables are fine enough and the value ranges are wide enough. The disadvantage of enumeration is that more computing time has to be spent with the number of design variables and discrete nodes of each variable increasing. Finally, the optimized full aerospike contour is truncated according to pressure distribution along full plug surface at design altitude and plug length restrictions.

3. Experimental apparatus

To validate the proposed aerospike nozzle contour design method, three different types of aerospike nozzles were design and manufactured. They were experimentally studied by either cold-flow tests or hot-firing tests. Propellants were supplied under pressure by a pressure-fed system. Highly pressurized air was employed as the propellant in cold-flow tests. The high pressure air supplying tanks can be pumped to 13 MPa, its maximum operational working mass flow rate is about 16 kg/s. In hot-firing tests, propellant feed system consists of gas oxygen and gas hydrogen in normal temperature. Propellants mass flow rate and mixing ratio are controlled by sonic nozzle after the propellants flowing from pressure regulators. Highly pressurized cold-flow gas nitrogen was employed as the puffing gas. The altitude simulation test system, with a total vacuum volume of more than 150 m^3, includes a testing vacuum vessel with diameter of $\varnothing$ 3.5 m, four large cylindrical vacuum exhaust tanks and vacuum pumps. The detonation wave igniter was adopted in hot-firing tests and three chambers were ignited by one igniter.

To obtain the performance of tested aerospike nozzles, thrust F, combustion chamber pressure P_c and ambient pressure in vacuum vessel P_a were measured. In addition, the measured parameters include several wall pressure data along plug ramp P_p, propellant pressure at engine head and pressure and temperature at different positions along propellant feed lines. The aerospike nozzle engines were fixed on test stand mounting horizontally in the test vessel. The test stand possesses automatic thrust force local calibrating system improving its precision and reliability. The error analysis reveals that the uncertainty of the entire thrust acquisition is less than 1.0% and the acquisition of pressure is more accurate than that of thrust. Thrust efficiency η was adopted to evaluate the performance of aerospike nozzles which is the ratio of experimental thrust coefficient C_F to the ideal one C_{F0} at a certain altitude [9]. $\eta = C_F/C_{F0}$, here $C_F = F/(P_c A_t)$, where A_t denote primary nozzle throat area. C_{F0} is computed as following

$$C_{F0} = \sqrt{\gamma}\left(\frac{2}{\gamma+1}\right)^{\gamma+1/2(\gamma-1)} \times \sqrt{\frac{2\gamma}{\gamma-1}\left[1-\left(\frac{1}{NPR}\right)^{\gamma-1/\gamma}\right]}$$

where nozzle pressure ratio $NPR = P_c/P_a$ is the indicator of altitude.

4. Numerical method

Because of the primary nozzle area ratio is small, the effects of ambient pressure on the flow in the primary nozzle can be neglected; therefore, the calculations of the internal flow for the primary nozzle and the external flow for the plug were done separately. The flow parameters at the primary nozzle exit were used as an inflow boundary condition for the plug flow. The governing equations are compressible three-dimensional Reynolds-averaged Navier–Stokes (N–S) equations. The values of the Reynold stresses and turbulent heat fluxes for N–S equations were obtained by the Lam–Bremhorst k–ε turbulence model [21]. Monotone upstream-centered scheme for conservation laws (MUSCL)-type approach [22] was employed for the discrete convective terms and second-order central differencing scheme was used for the viscous terms. Only the steady-state solutions were considered and an implicit lower–upper (LU) diagonal decomposition algorithm [23] was employed. The effects of the external flow were not considered and details dealing with boundary conditions and the turbulence model can be found in Ref. [24].

5. Tile-shaped aerospike nozzle test

5.1. 6-Cell tile-shaped aerospike nozzle

As shown in Fig. 5, each primary nozzle of the 6-cell tile-shaped aerospike nozzle is a bell-shaped nozzle with small area ratio. The primary nozzle throat diameter is $D_t = \varnothing$ 14 mm and its inclination is $\alpha = 30^\circ$. The width of the aerospike nozzle is $W = 114$ mm. The area ratios of the primary nozzle and overall aerospike nozzle are $\varepsilon_c = 4$ and $\varepsilon_{all} = 40$, respectively. Complete expansion is achieved at $NPR = 1046$.

In order to compare the performance of aerospike nozzle with bell-shaped nozzle, a bell-shaped nozzle was fabricated and tested (see Fig. 6). The contour of bell-shaped nozzle for comparing was designed by characteristic method and inner wall of the nozzle was manufactured smoothly enough. Its throat diameter is $D_t = \varnothing$ 26 mm and its area ratios is $\varepsilon_{all} = 40$. For this area ratio, optimum expansion is also achieved at $NPR = 1046$. Its design point is the same with that of the 6-cell tile-shaped aerospike nozzle.

5.2. Results and discussion

Fig. 7 shows the measured thrust efficiencies of 6-cell tile-shaped aerospike nozzle and bell-shaped nozzle as

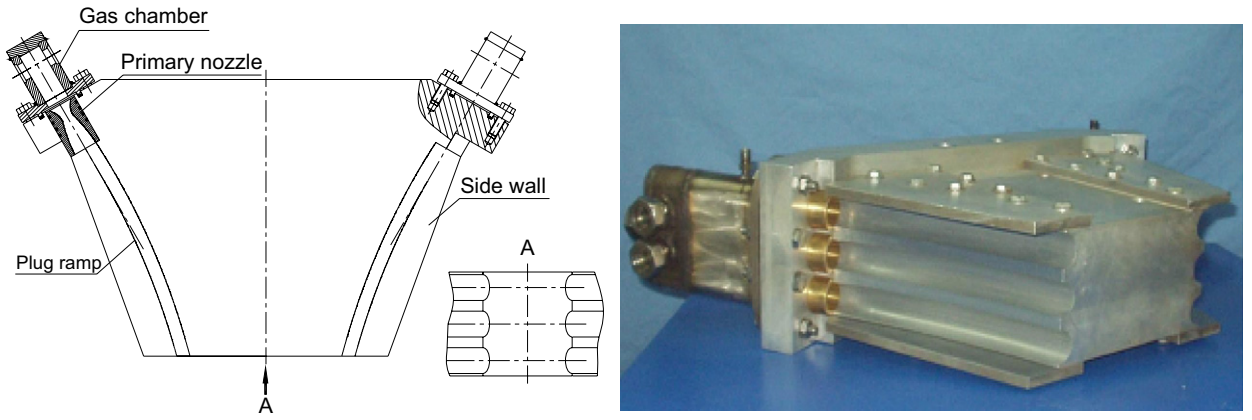

Fig. 5. Sketch and photograph of 6-cell tile-shaped aerospike nozzle.

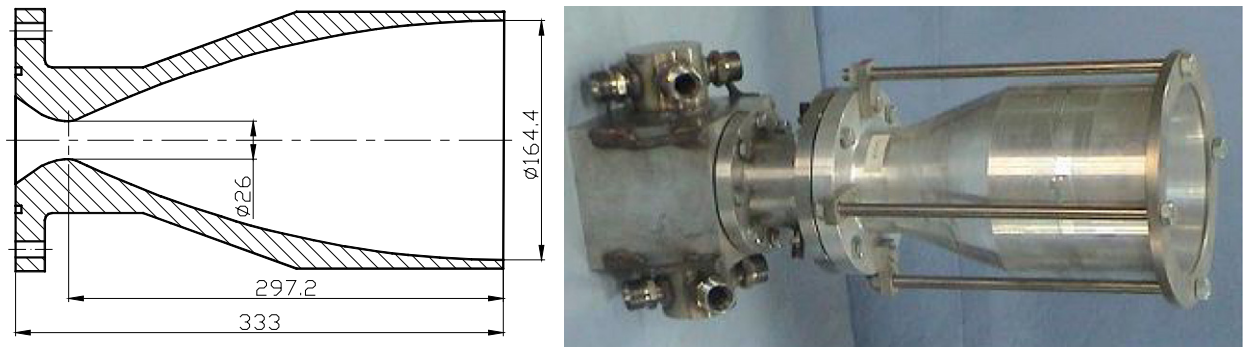

Fig. 6. Sketch and photograph of bell-shaped nozzle for comparison.

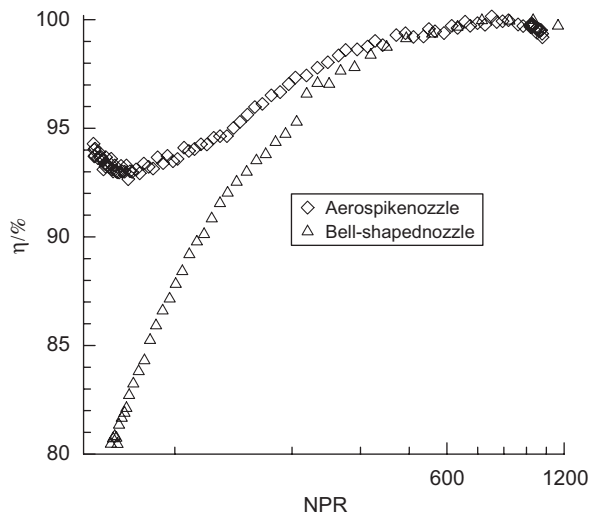

Fig. 7. Efficiencies of aerospike nozzle and bell-shaped nozzle as a function of *NPR*.

a function of *NPR*. When *NPR*s are more than 400, the altitude characteristics of the aerospike nozzle coincide with that of bell-shaped nozzle and 400 is also the minimum *NPR*, from which the pressure distribution along the plug is not changed any more. It is shown that the expansion characteristics of the aerospike nozzle appear analogous to that of the bell-shaped nozzle after $NPR = 400$ and from $NPR = 400$ on, the pressure distribution along the plug is similar to that along the inner wall of the bell-shaped nozzle. At the design *NPR*, both the aerospike nozzle and bell-shaped nozzle obtained high thrust efficiency. However, at *NPR*s lower than the design value, the aerospike nozzle has good capacity of altitude compensation compared with the bell-shaped nozzle and still shows higher performance at off-design altitudes. From sea level to design altitude, efficiencies of the aerospike nozzle and bell-shaped nozzle varied within the range of 93.0–100.0% and 66.0–100.0%, respectively. The remarkable performance gain of the aerospike nozzle was 27.0% compared with the conventional nozzle at sea level. By comparison of present experimental results and that obtained with cylindrical tile-shaped aerospike nozzle in Ref. [13], it is concluded that simplified plug contour (cylindrical plug)

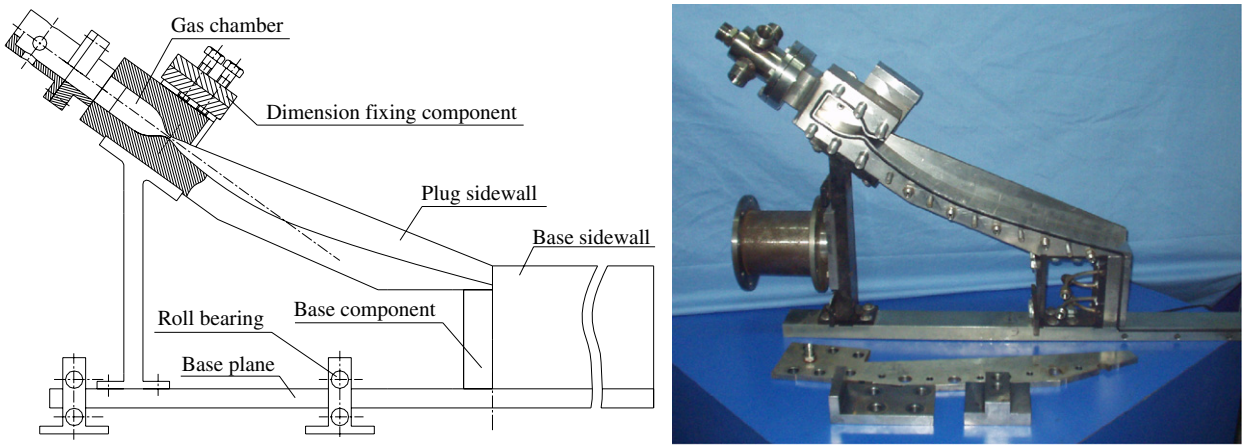

Fig. 8. Sketch and photograph of 1-cell linear aerospike nozzle.

may cause several percent of performance losses. It was shown by measured data comparison that tile-shaped aerospike nozzle has inherent thrust compensability and better aerodynamic performance than bell-shaped nozzle.

6. Linear aerospike nozzle test

6.1. 1-Cell linear aerospike nozzle

The 1-cell linear aerospike nozzle is shown in Fig. 8. The width of the aerospike nozzle is $W = 60$ mm, the height of the throat is $D_t = 4.09$ mm and the primary nozzle inclination is $\alpha = 35.9^\circ$. The area ratios of the primary nozzle and overall aerospike nozzle are $\varepsilon_c = 4$ and $\varepsilon_{all} = 80$, respectively. Complete expansion is achieved at $NPR = 2840$. Six pressure transducer ports were placed along plug surface. Derived from the primary nozzle gas chamber, some amount of the total mass flow rate is injected into the base region through uniformly distributed 366 holes with diameter of $\varnothing$ 1 mm. Tests were conducted under the six conditions of 0.0, 1.0, 1.5, 2.0, 3.0 and 4.0% base bleed ratios, which is the ratio of mass flow rate injected into the base region to the total mass flow rate in gas chamber.

6.2. Results and discussion

Figs. 9a and b show the measured thrust efficiencies of the 1-cell linear aerospike nozzle with the base bleed ratios varying from 0.0% to 4.0% as a function of *NPR*. The performances with different base bleed ratios are almost the same when the base wake is open. It is shown that under open wake condition, the base bleed injection does not exert an obvious influence on the aerospike nozzle efficiency. With the base bleed ratio increasing, three differences in altitude characteristics were observed. The first one is the extents to which the efficiencies were degraded are different at the base transitions from open to close. The second one is the *NPR*s at which the base transitions take place are different. The third one is performances are different under close wake condition and at design *NPR*. In the case of without base bleed (0.0%), notable efficiency degradation was observed at the base transition (near $NPR = 140$) and the efficiency reduced from 89.0% (in open wake condition) to 82.3% (in close wake condition). The aerodynamic transition of the base behavior contributes to the performance degradation and results in remarkable change of the thrust. When some base bleed was injected, sharp decrease of performance reduction at base transition was observed. The efficiency reduction at base transition decreased from 3.2% to 0.12% with the base bleed ratios from 1.0% to 4.0%. When more than 2.0% the base bleed ratio was injected, no remarkable performance reduction occurred at base transition.

The tested aerospike nozzle had the highest efficiency at design *NPR* in case of 1.0% and 1.5% base bleed ratios. Performances in case of 0.0% and 2.0% base bleed ratios were similar, but a little lower than that in 1.0% and 1.5% base bleed ratios cases. Performances with 3.0% and 4.0% base bleed ratios were further lowered compared with former cases, especially in case of 4.0% base bleed ratio. The base pressure is increased and the performance degradation at base transition is avoided due to some base bleed injection. However,

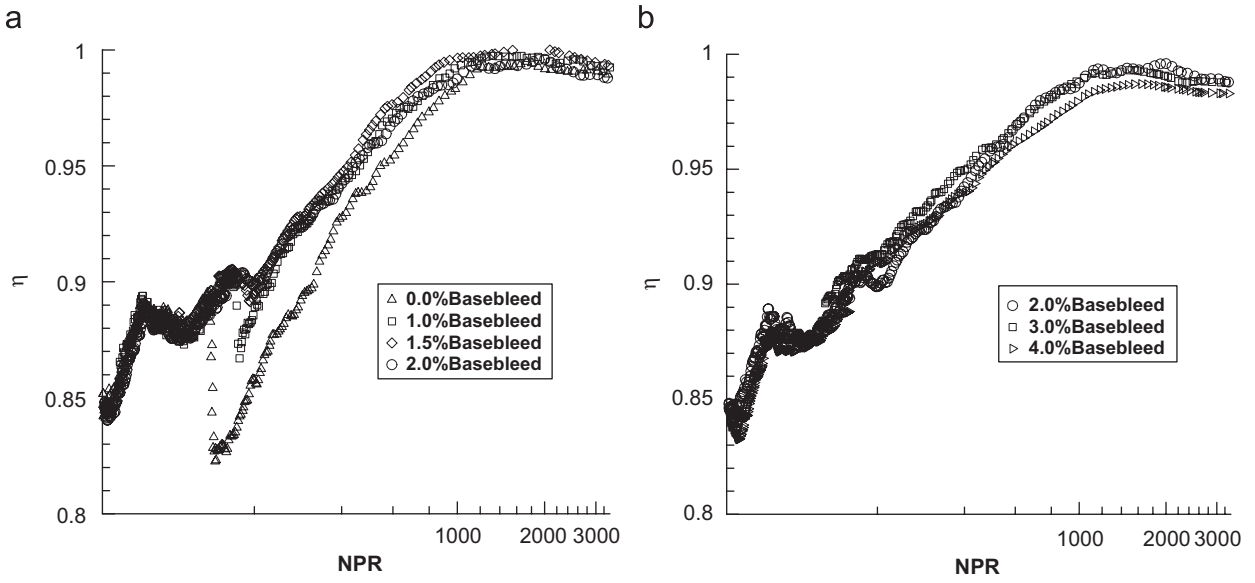

Fig. 9. Test aerospike nozzle efficiency as a function of *NPR*: (a) 0.0–2.0% base bleed ratios and (b) 2.0–4.0% base bleed ratios.

too much bleed injection results in overall performance degradation, especially at design *NPR*. 1.5–2.0% base bleed injection seems to be the best in the test.

Fig. 10 shows measured pressure profiles along 1-cell linear aerospike nozzle plug ramp in length x direction. The influence of the ambient pressure on aerospike nozzle flowfield can be seen obviously from pressure distribution under different *NPR*s. At low altitudes, flow follows the course of expansion–compression–expansion and fluctuated pressure was obtained along plug ramp surface. As the ambient pressure decreasing, the influence of the ambient pressure on aerospike nozzle flowfield becomes weaker that is the pressure amplitudes become smaller and the pressure rising positions move rearward. It is shown that the influence of the back pressure moved out of the plug ramp surface eventually and the pressure distribution along the plug surface was no longer changed at *NPR*s more than 300.

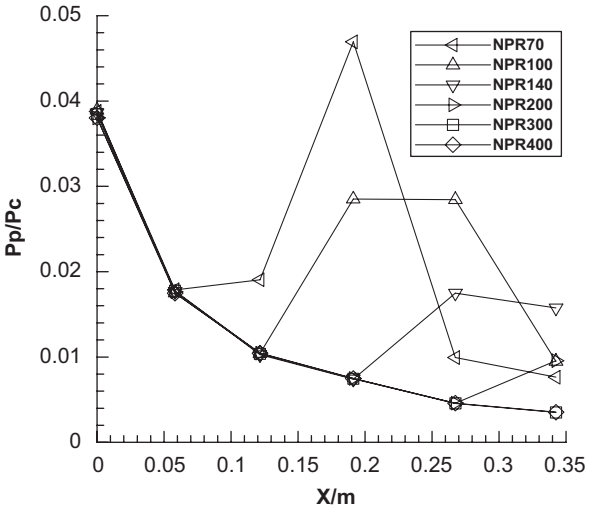

Fig. 10. Experimental pressure distribution along a plug ramp.

7. Aerospike nozzle with RTR primary nozzles test

7.1. 3-Cell aerospike nozzle with RTR primary nozzles

As shown in Fig. 11, the hot-firing tested engine is a 3-cell aerospike nozzle engine. The engine mainly comprises three primary nozzle thrust chambers and a plug ramp. The distance between two adjacent primary nozzles is 66 mm. The primary nozzle inclination is $\alpha = 37.5^\circ$ and the width of the plug ramp is $W = 200$ mm. The overall aerospike nozzle are $\varepsilon_{all} = 80$, achieving complete expansion at $NPR = 1139$.

As shown in Fig. 12, the primary nozzle is a RTR nozzle whose throat diameter is $D_t = \varnothing 16$ mm and area ratio is $\varepsilon_c = 5.77$. The transition from the round cross section to the rectangle with round corners exit cross section starts at the area ratio of $\varepsilon = 1.38$. The radii of the round corners change smoothly from $R_1 = 9.4$ mm at starting section to $R_2 = 10.0$ mm at exit section.

As is shown in Fig. 13, three coaxial gas H_2/gas O_2 (GH_2/GO_2) injector elements in the injector are distributed along a circle with diameter of $\varnothing 24$ mm. Four gas hydrogen inlets with diameter of $\varnothing 20$ mm

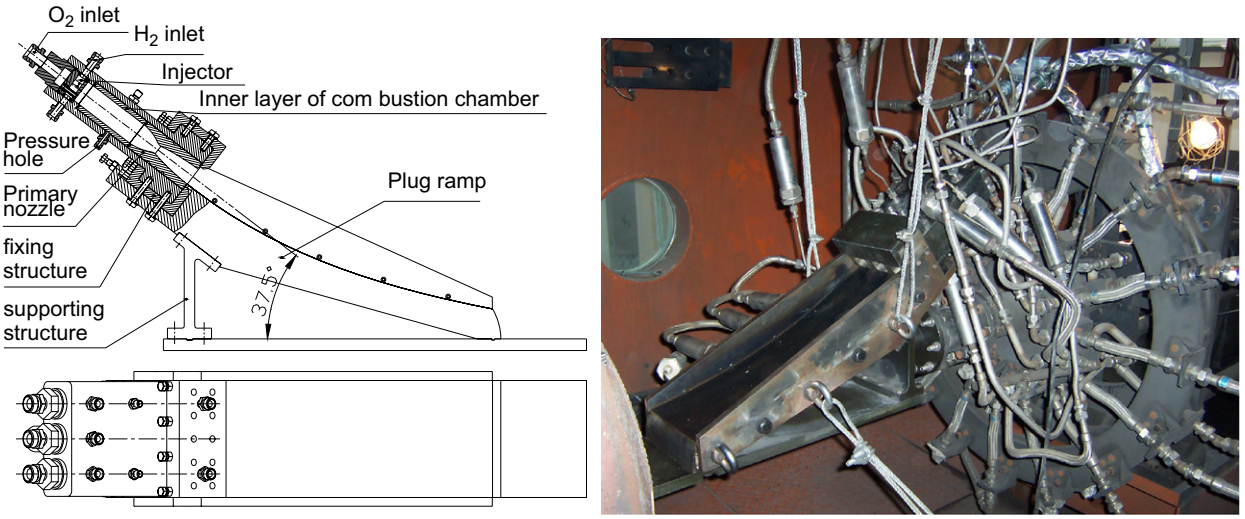

Fig. 11. Sketch and photograph of 3-cell aerospike nozzle with round-to-rectangle primary nozzles.

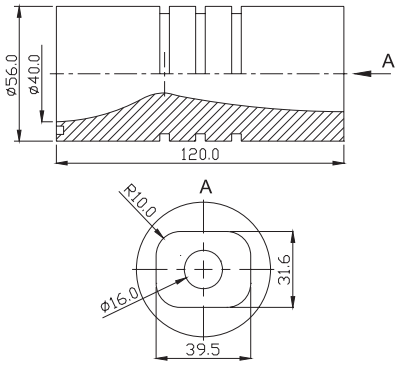

Fig. 12. Sketch of RTR primary nozzle.

Fig. 13. Photograph of injector and its injector elements.

distribute along tangential direction of the injector cylinder. Sketch of GH_2/GO_2 injector element is shown in Fig. 14. The outer diameter of gas oxygen injector element is ∅6 mm and its internal diameter is ∅3.6 mm. The outer diameter of gas hydrogen injector element is ∅8 mm and its internal diameter is ∅6.8 mm. Six gas hydrogen inlets holes with diameter of ∅2 mm distribute along tangential direction of the gas hydrogen injector element. Gas hydrogen flowing channel is an annular gap area with internal diameter of ∅6 mm and outer diameter of ∅6.8 mm. The retractive distance from the end of gas hydrogen injector element to the end of gas oxygen injector element is 2 mm. The 36 little holes with diameter of ∅1.0 mm distributing along three circles are drilled in injector plate to jet gas hydrogen for thermal protection.

Under design condition the engine parameters are illustrated in Table 1.

7.2. Results and discussion

Two hot-firing tests were carried out on 3-cell aerospike nozzle engine under two different ambient pressure conditions. In the tests, three thrust chambers were successfully ignited by the detonation wave igniter. And the injector parameters, such as β, hydrogen injector pressure drop ΔP_H and oxygen injector pressure drop ΔP_O are shown in Table 2.

Fig. 15 shows the test results near $NPR = 350$ as an example, illustrating the measured data of engine thrust F and three pressures in combustion chambers P_{c1}–P_{c3}. Engine thrust and pressure in combustion chambers achieve 3500 N and 3.4 MPa, respectively, when their values reach steady states. Three combustion chamber pressure data have a good repetition in tests. Data at low NPR were obtained near $NPR = 50$ which is analogous to that shown in Fig. 15. The steady-state value of

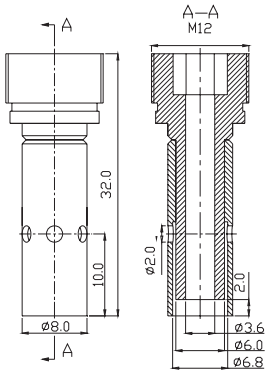

Fig. 14. Sketch of GH_2/GO_2 injector elements.

Table 1
Engine parameters under design condition.

Parameter	Value
Mixing ratio β	5.46
Combustion chamber pressure P_c	3.85 MPa
Combustion chamber temperature T_c	3427 K
Specific heat ratio γ	1.198
Gas constant R_g	632.0 J/kg K
Total flow rate $\dot{m}_{all}$	0.901 kg/s

Table 2
Parameters of the injector in the tests.

Case	β	ΔP_H (MPa)	ΔP_O (MPa)
1	5.62	0.29	1.26
2	5.36	0.35	1.25

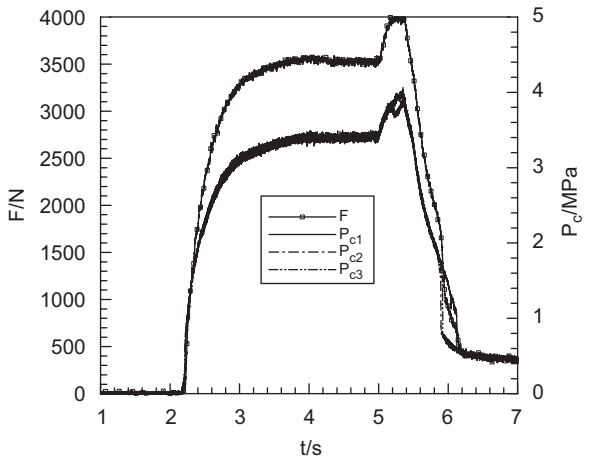

Fig. 15. Measured data in hot-firing test ($NPR = 350$).

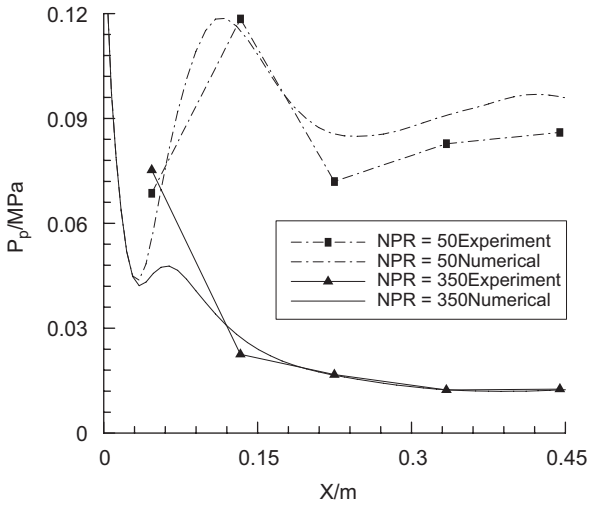

Fig. 16. Experimental and numerical pressure distribution along plug ramp.

engine thrust and combustion chamber pressure achieved 3000 N and 3.4 MPa, respectively. Both the magnitude of combustion chamber pressure in two tests were lower than its design value of 3.85 MPa.

Fig. 16 shows measured and numerical simulated pressure distribution along 3-cell aerospike nozzle plug ramp in length x direction. At $NPR = 50$, fluctuated pressure profiles were obtained along plug ramp surface and this high pressure compensated the nozzle thrust which called altitude compensability made contribution for higher performance even at low altitudes. At $NPR = 350$, pressure along the plug ramp was monotonously decreased with flow expanding along plug surface, similar to that along the inner wall of the bell-shaped nozzle. The numerical results predicted the experimental data under corresponding *NPR*s on the whole.

Fig. 17 shows the measured and numerical simulated performance of 3-cell aerospike nozzle engine as a function of *NPR*. Thrust efficiencies at $NPR = 50$ and 350 were obtained from measured data in two tests. Near $NPR = 50$, efficiency is 92.0–93.5% and near $NPR = 350$, efficiency is 95.0–96.0%. The numerical simulated efficiency is in good agreement with the test result at $NPR = 350$. The computed efficiency is about 90.0% at $NPR = 50$, however, the measured value varies within the range of 92.0–93.5%, several percent lower than theoretical prediction. Because the characteristic of aerospike nozzle, generally speaking, the numerical simulation precision at lower *NPR* is not as good as that at higher *NPR*.

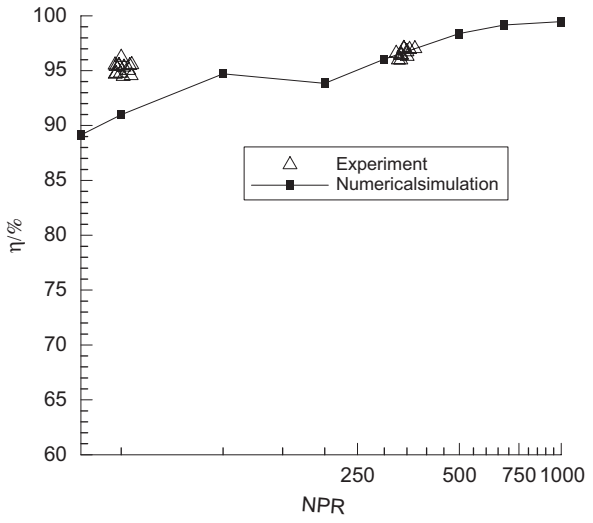

Fig. 17. Aerospike nozzle efficiency as a function of *NPR*.

8. Conclusions

Based on the curvefitting analysis of the contours designed by Angelino method, a full aerospike nozzle contour described approximately by simple geometric curves is proposed, namely, two circular arcs and a parabola for the primary nozzle contour and a parabola and a third-order polynomial for the plug contour. All these curves connect with each other smoothly and their geometry can be determined by geometric and aerodynamic restrictions. The plug contour designed by the proposed method almost coincides with that designed by Angelino method and this modeling makes it simple to design and optimize the aerospike nozzle contours. Design methods of the tile-shaped plug and the RTR primary nozzle are also presented. The maximum total impulse from sea level to design altitude is selected as an objective and optimum design parameters are obtained by the computation and comparison of enumeration of the discrete values of the design variables.

Both experimental and numerical studies were performed on a 6-cell tile-shaped aerospike nozzle, a 1-cell linear aerospike nozzle and a 3-cell aerospike nozzle with RTR primary nozzles designed by method proposed in the paper. Three aerospike nozzles achieved good altitude compensation capacities in the tests and still had better performance at off-design altitudes compared with that of the bell-shaped nozzle. In cold-flow tests, 6-cell tile-shaped aerospike nozzle and 1-cell linear aerospike nozzle obtained high thrust efficiency at design altitude. Employing GH_2/GO_2 as propellants, hot-firing tests were carried out on a 3-cell aerospike nozzle engine with RTR primary nozzles. The performance was obtained under two nozzle pressure ratios lower than design altitude. Near $NPR = 50$, efficiency is 92.0–93.5% and efficiency is 95.0–96.0% near $NPR = 350$. The promising efficiency of more than 98.0% at design point can be expected. Pressure distribution along plug ramp was measured and the effects of variation in the amount of base bleed on performance were also examined in the tests. Experimental data validate the proposed aerospike nozzle contour design and optimization method.

Acknowledgment

Experimental work has been performed by all members of the aerospike nozzle research team. The authors would like to acknowledge Ph.D. Yun-Fei Liao, Jun-Wei Li and Yi-Bai Wang for their contributions in the experiments.

References

[1] H.M. Ryan, W. Solano, R. Holland, et al., The future of full-scale propulsion testing, AIAA-2001-0746, 2001.
[2] A.W. Stephen, R.M. Timothy, A base drag reduction experiment on the X-33 linear aerospike SR-71 experiment (LASRE) flight program, AIAA-99-0277, 1999.
[3] M. Onofri, Plug nozzles: summary of flow features and engine performance, AIAA-2002-0584, 2002.
[4] T. Tomita, M. Takahashi, H. Tamura, Flow field of clustered plug nozzles, AIAA-97-3219, 1997.
[5] H. Sakamoto, M. Takahashi, M. Sasaki, et al., An experimental study on a 14 kN linear aerospike nozzle combustor, AIAA-99-2761, 1999.
[6] S.V. Baftalovskii, A.N. Kraiko, N.I. Tillyayeva, Optimal design of self-controlled spike nozzles and their thrust determination at start, AIAA-99-4955, 1999.
[7] G.E. Dumnov, G.Z. Nikulin, N.B. Ponomaryov, Investigation of advanced nozzles for rocket engines, Space Rocket Engines and Power Plants 4 (1993) 142 (in Russian).
[8] C.H. Wang, Experimental and Numerical Investigation of Aerospike Nozzle Aerodynamic Characteristics, Beijing University of Aeronautics and Astronautics, Beijing, 2005 (in Chinese).
[9] H. Mori, M. Taniguchi, R. Nishihira, et al., Experimental analyses of linear-type aerospike nozzles with and without sidewalls, AIAA-2005-1350, 2005.
[10] W.Y. Dai, Y. Liu, X.C. Cheng, et al., Aerospike nozzle performance study and its contour optimization, AIAA-2001-3237, 2001.
[11] Y. Liu, G.Z. Zhang, W.Y. Dai, et al., Experimental investigation on aerospike nozzle in different structures and working conditions, AIAA-2001-3704, 2001.
[12] W.Y. Dai, Y. Liu, X.C. Cheng, et al., Numerical and experimental study of tile-shaped aerospike, AIAA-2002-4035, 2002.

[13] W.Y. Dai, Y. Liu, X.C. Cheng, et al., Analytical and experimental studies of tile-shaped aerospike nozzles, Journal of Propulsion and Power 19 (4) (2003).
[14] C.H. Wang, Y. Liu, L.Z. Qin, et al., Performance analysis of linear clustered aerospike nozzles, Journal of Beijing University of Aeronautics and Astronautics 30 (7) (2004) 627–630 (in Chinese).
[15] C.H. Wang, Y. Liu, Studies on base pressure model of aerospike nozzle, Chinese Journal of Aeronautics 26 (1) (2005) 5–9 (in Chinese).
[16] C.H. Wang, Y. Liu, Effects of free stream on flowfield and performance of linear aerospike nozzle, Journal of Beijing University of Aeronautics and Astronautics 32 (2) (2006) 130–134 (in Chinese).
[17] G. Angelino, Approximate method for plug nozzle design, AIAA Journal 2 (10) (1964).
[18] H. Immich, M. Caporicci, Status of the FESTIP rocket propulsion technology program [R]. AIAA 97–3311, 1997.
[19] T. Tomita, H. Tamura, M. Takahshi, An experimental evaluation of plug nozzle flow field, AIAA-96-2632, 1996.
[20] J.G. Allman, J.D. Hoffman, Design of maximum thrust nozzle contours by direct optimization methods, AIAA-78-1048, 1978.
[21] C.K.G. Lam, K.A. Bremhorst, Modified form of the k–ε model for predicting wall turbulence, Journal of Fluids Engineering 103 (3) (1981) 456–460.
[22] B. Van Leer, Towards the ultimate conservative difference scheme V: a second-order sequel to Godunov's method, Journal of computational Physics 32 (1979) 101–136.
[23] J.S. Shuen, S. Yoon, Numerical study of chemically reacting flows using a lower–upper symmetric successive overrelaxation scheme, AIAA Journal 27 (12) (1989) 1752–1760.
[24] C.H. Wang, Y. Liu, The effects of primary configurative parameters on the performance of linear aerospike nozzles, Journal of Propulsion Technology 25 (5) (2004) 439–443 (in Chinese).